Anal. Bioanal. Electrochem., Vol. 16, No. 5, 2024, 389-404
https://www.doi.org/10.22034/abec.2024.713500

Analytical & Bioanalytical Electrochemistry

Full Paper

Green Synthesis of CuO-ZnO Nanocomposite using Citrus Sinensis Fruit Peel Extract for Electrochemical Detection of Hydrogen Peroxide

Megersa Gudisa Bulcha, Ebisa Mirete Deresa, Gebru Gebretsadik, Guta Gonfa,* and Shimeles Addisu Kitte*

Department of Chemistry, College of Natural Sciences, Jimma University, P.O. Box 378, Jimma, Ethiopia

*Corresponding Author, Tel.: +251-923345768 (G. Gonfa); +251-966153015 (S.A. Kitte)
E-Mails: guta.gonefa@ju.edu.et (G. Gonfa); shimeles.addisu@ju.edu.et (S.A. Kitte)

Received: 29 July 2023 / Received in revised form: 20 May 2024 / Accepted: 21 May 2024 / Published online: 31 May 2024

Abstract- In this work, CuO nanoparticles (NPs), ZnO NPs, and CuO-ZnO nanocomposites (NCs) were synthesized using Citrus sinensis fruit peel extract. Then, carbon paste electrodes modified with each nanomaterial (CuO-CPE, ZnO-CPE, and CuO-ZnO-CPE) was fabricated for the electrochemical detection of hydrogen peroxide (H2O2). The prepared metal oxide nanomaterials were characterized using Ultraviolet-Visible (UV-Vis) spectroscopy, Fourier transform infrared (FT-IR) spectroscopy, X-ray diffraction (XRD), and scanning electron microscopy (SEM). The average crystallite sizes for nanomaterials composed of CuO and ZnO NPs and CuO-ZnO NCs were 32.2 nm, 31.7 nm, and 35.38 nm, respectively. A carbon paste electrode modified with CuO-ZnO NCs (CuO-ZnO-CPE) was used to detect H2O2. At CuO-ZnO-CPE, a cathodic peak for H2O2 was seen at about 0.0 V. Under optimum experimental conditions, the developed electrode showed a wide linear range from 0.5 µM to 200.0 µM with a limit of detection (LOD) of about 0.32 µM. The synthesized electrode also showed increased stability, adequate selectivity, and repeatability.

Keywords- Citrus sinensis; CuO nanoparticles; ZnO nanoparticles; CuO-ZnO nanocomposite; Electrochemical detection; Hydrogen peroxide

1. INTRODUCTION

Hydrogen peroxide (H_2O_2) is a vital substance for different applications, such as in medical, pharmaceutical, environmental and industry [1]. In addition to its ability to be a powerful oxidizing agent, it is also one of the by-products of various oxidation reactions, which has the potential to contaminate the environment [2, 3]. Numerous studies have shown that high levels of H_2O_2 adversely affect the body's physiological processes and can lead to a number of illnesses in a live creature, including cancer, tumors, Alzheimer's, and Parkinson's disease [4]. Hence, there is a great deal of interest in creating a quick, inexpensive, accurate, and selective method for H_2O_2 detection. H_2O_2 has been detected using a variety of techniques, such as chemiluminescence [5], fluorescence [6], spectrophotometry [7], and electrochemistry [8]. Due to its high sensitivity, easy operation, and quick detection, electrochemistry has garnered the most interest among these techniques [9].

Electrochemical sensors based on nanomaterials usually show large specific surface areas, exceptional conductivities, remarkable electrocatalytic activities, thermal stability, irradiation resistance, and a propensity to produce diverse nanostructures [10]. When compared to conventional alternatives like enzymatic biosensors, these nanomaterials have proven to function better. In addition, compared to their precursor nanoparticles, nanocomposites (NCs) have favorable and distinctive traits because of their enhanced physical and chemical properties, large surface area, increased ability to transmit electrons, and unique optical qualities [11]. It is commonly recognized that the unique properties of nanomaterials are determined by their structure and surface morphology [10]. The nanomaterial's conductivity, adsorption efficiency, and electrocatalytic activity are all significantly influenced by its phase purity and crystallinity [12].

Previously, electrochemical detection of H_2O_2 was studied using different nanomaterials as electrode modifiers. Some of the nanomaterials employed in previous investigations include Fe_3O_4/Graphene/Carbon Cloth (Fe_3O_4/Gr/CC) nanocomposite [11], diamond nanoparticles on glassy carbon (GC/DNp) or gold surfaces (Au/DNp), and copper nanoparticles electrochemically generated directly on glassy carbon surfaces (GC/CuNp) [13], a glassy carbon electrode modified with palladium film and palladium nanoparticle [3], a glassy carbon electrode modified with ionic liquid crystal (ILC), carbon nanotubes (CNTs) and Fe-Ni alloy nanoparticles (GC/ILC/(CNT-Fe-Ni) [14], graphene nanoribbons/Cobalt oxide nanorods (GNR/Co_3O_4) nanocomposite [15], Prussian Blue electrodeposited at a glassy carbon (GC) electrode modified with titanium dioxide and zirconia-doped functionalized carbon nanotubes (PB/TiO_2.ZrO_2-fCNTs/GC) [16], and a glassy carbon electrode modified with Fe-Cu layered double hydroxide (LDH)/magnetic Fe_3O_4 nanoparticles (FeCu-LDH@Fe_3O_4/GCE) [17].

Metal oxide nanomaterials, for instance, CuO and ZnO nanoparticles (NPs) [18,19] synthesized via the green method using plant extracts have enormous potential in the development of electrochemical biosensors. The demonstration of an effective green synthesis

method using plant extract as an easy and alternative approach for chemical and physical techniques to prepare metal oxide nanoparticles has become researchers' main focus [20]. Tannins, terpenoids, phenols, alkaloids, phenolic acids, and saponins are commonly found in plant extracts and are in charge of converting the metal ions into their reduced form during the synthesis of metal oxide nanoparticles and stabilizing them [21,22]. Researchers have been paying close attention to using nanomaterials derived from plants for the electrochemical detection of H_2O_2 in recent years. One study, for instance, used ZnO NPs made from *Corymbia citriodora* leaf extract to detect H_2O_2 electrochemically [23]. Apart from this, silver nanoparticles (AgNPs) synthesized from *Durio zibethinus* rind extract [24], silver nanoparticles modified carbon paste electrode (CPE) fabricated using *Acacia melanoxylon* leaves extract [25], and palladium doped reduced graphene oxide composite (Pd@rGO) synthesized using *Onosma malatyana* roots extract [26] were investigated for electrochemical detection of H_2O_2.

The CPE has been widely used as an electrode for the determination of various electroactive chemicals because of its special qualities, which include low cost, outstanding electrical properties, large potential windows, and renewability of the electrode surface [27]. Apart from the intriguing characteristics already described, the capacity to alter CPE through the use of various modifiers has been applied widely to enhance the electron transfer process for sensitive electroactive species identification [28]. Modified CPEs are commonly used for sensitive assessments of trace levels of heavy metals [29], physiologically relevant chemicals [30], pharmaceuticals [31], and other substances.

In this study, we present a novel environmentally friendly method that uses an aqueous extract of *Citrus cinensis* fruit peel to synthesize ZnO NPs, CuO NPs, and CuO-ZnO NCs. Utilizing UV-Vis, FT-IR, XRD, and SEM, the fabricated CuO NPs, ZnO NPs, and CuO-ZnO NCs have been characterized. Using the prepared CuO-ZnO NCs as carbon paste electrode modifiers, we investigated the electrochemical detection of H_2O_2.

2. MATERIALS AND METHODS

2.1. Chemicals and reagents

Zinc nitrate hexahydrate (98% purity), copper nitrate (Laboratory reagent, 99%), sodium hydroxide (pure pellet, 99%), acetic acid, ethanol (Analytical reagent, 99.9%), hydrogen peroxide (30%, Aldrich), potassium bromide, potassium dihydrogen phosphate (99%, NICE), dipotassium phosphate (98%, FINKEM), hydroquinone (HQ), ascorbic acid (AA), dopamine (DA), uric acid (UA), distilled water, ferric chloride, ammonia, concentrated sulphuric acid, iodine, potassium iodide was used in this study. All chemicals and reagents used were of analytical grade. Analytical grade chemicals and reagents were utilized in every instance.

2.2. Instruments and apparatus

UV-Vis spectrophotometer (PerkinElmer Lambda 25), FT-IR spectroscopy (PerkinElmer Spectrum Two), XRD (Drawell XRD 7000), SEM (SU3500N), voltammetry analyzer (Epsilion EC-Ver 1.40. 67) were used in this work.

2.3. Preparation of *Citrus sinensis* fruit peel extract

Citrus sinensis fruit was purchased from a market in Jimma town, Ethiopia. The fruit was rinsed with plenty of distilled water, peeled and juice removed from the peel and then the peel was chopped into small pieces. The peel was ground into a reasonably fine powder after being shade-dried. 25 mL distilled water was added to an Erlenmeyer flask containing 3 g of powder and heated with stirring on a hot plate for 30 min. The peel extract was filtered through Whatman No. 1 filter paper, and the extract solution was then refrigerated at 4°C until the subsequent experiment [32].

2.4. Phytochemical screening tests

Qualitative phytochemical screening tests for phenols, tannins, flavonoids, alkaloids, and saponins were performed following the standard methods already reported [7-9]. 3 drops of a 5% Ferric chloride solution were added to 1 mL of extract for testing the presence of phenols and tannins. The development of a bluish-black color was indicative of the presence of tannins and/or phenols [33]. For flavonoids, 1 mL of extract solution was mixed with 5 drops of diluted ammonia. 1 mL of concentrated sulfuric acid was then added to the mixture. The formation of a yellow color that vanished upon standing was a sign that flavonoids were present [9]. For alkaloids, 1 mL of the extract solution was mixed with 5 drops of Wagner's reagent (1.27 g of iodine and 2 g of potassium iodide in 100 mL of distilled water). The presence of alkaloids was detected by the development of a reddish-brown precipitate [32]. A 1 mL extract solution was agitated with 2 mL distilled water to extract saponins. For testing saponins, 1 mL extract solution was treated with 2 mL distilled water. The presence of saponins was indicated by the formation of bubbles (foam) [34].

2.5. Preparation of CuO NPs, ZnO NPs and CuO-ZnO NCs

CuO NPs, ZnO NPs, and CuO-ZnO NCs were prepared using *Citrus sinensis* fruit peel extract as a reducing and capping agent and copper nitrate and zinc nitrate as precursors. ZnO NPs were prepared by mixing 50 mL of 0.18 M $Zn(NO_3)_2$ solution with 15 mL of *Citrus sinensis* fruit peel extract and adding 0.2 M NaOH until the pH reaches 10. A white precipitate appeared after 4 hours of stirring the solution at 80 °C. To get rid of contaminants, the prepared white precipitate was filtered through Whatman No. 1 filter paper and repeatedly rinsed with ethanol and distilled water. The same approach was used for the synthesis of CuO NPs except

using 50 mL of 0.09 M $Cu(NO_3)_2$ as precursor [35]. For synthesis of CuO-ZnO NCs, 50 mL of 0.18 M $Zn(NO_3)_2$ was first added to 15 mL of fruit peel extract and then mixed with 10 mL of 0.2 M NaOH. After 2 h of heating at 80 °C with continued stirring, 25 mL of 0.09 M $Cu(NO_3)_2$ was poured into the solution and the mixture was heated at 80 °C for additional 4 h. After forming a greenish precipitate, it was filtered using Whatman filter paper, repeatedly cleaned with ethanol and distilled water to get rid of contaminants, and then dried for 24 hours at 80 °C in an oven [36].

2.6. Characterization of nanomaterials

The prepared nanomaterials were characterized using a number of methods, including UV-Vis, FT-IR, XRD, and SEM. These methods showed a variety of properties, including band gap, functional groups, size, and surface morphology, respectively.

2.7. Electrode preparation and procedure for electrochemical sensing

2.7.1. Preparation of unmodified carbon paste electrode (UCPE)

By mixing 20% (w/w) paraffin oil and 80% (w/w) graphite powder, UCPE was prepared. The mixture was homogenized for 30 minutes using a mortar and pestle, and then let to rest for 24 hours. A Teflon tube (3 mm in diameter and 7 mm depth) is used to package the homogenized paste. A copper wire was introduced from the reverse side of the Teflon tube to establish electrical contact. After that, the electrode's surface was polished until a smooth surface emerged against a piece of white paper that was smooth [37].

2.7.2. Preparation of the Modified Carbon Paste Electrodes

CuO-ZnO NCs modified carbon paste electrode (CuO-ZnO-CPE) was prepared by mixing 65% (w/w) graphite powder, 20% (w/w) paraffin oil, and 15% (w/w) CuO-ZnO NCs. The same proportion was used to prepare CuO NPs modified carbon paste electrode (CuO-CPE) and ZnO NPs modified carbon paste electrode (ZnO-CPE). A Teflon tube (3 mm in diameter and 7 mm depth) is used to package the homogenized paste. From the reverse side of the Teflon tube, a copper wire was introduced to establish electrical contact. Next, a smooth piece of paper was used to polish the electrode's surface until a smooth surface was achieved [37].

3. RESULTS AND DISCUSSION

3.1. Qualitative Tests for Preliminary Phytochemical Screening

Phytochemical screening tests are simply chemical tests used to identify classes of phytoconstituents present in plant extract. In the green synthesis of nanoparticles, the aim of these tests is to identify the types of phytochemicals playing the key role of reducing and capping agents [38]. The result of this test, as illustrated in Table 1, shows the presence of

phenols, tannins, flavonoids, alkaloids, and saponins in *Citrus sinensis* fruit peel aqueous extract. This result indicates that these phytochemicals are responsible for the bioreduction of the metal ions during the synthesis and stability of the nanoparticles. Each class of phytochemicals forms a characteristic color in the presence of the test reagent and if such color change does not occur, it indicates the absence of that phytoconstituent. In this study, the tested phytochemicals have been detected as indicated by the positive sign (+) in Table 1.

Table 1. The qualitative analysis of phytochemicals in the *Citrus sinensis* fruit peel extract

Phytochemicals	**Chemical test**	**Result**	**Colors observed**
Phenols	Ferric chloride test	+	Blue
Tannins	Ferric chloride test	+	Greenish black
Flavonoids	Dilute ammonia and concentrated sulfuric acid	+	Yellow
Alkaloids	Wagner's test	+	Reddish brown
Saponins	Distilled water	+	Layer of foam

3.2. Characterizations of the synthesized CuO NPs and ZnO NPs, CuO-ZnO NCs

UV-Vis spectrophotometer is used to determine the band gap of the prepared CuO NPs, ZnO NPs and CuO-ZnO NCs. The UV-Vis absorbance of the synthesized CuO NPs, ZnO NPs and CuO-ZnO NCs were recorded in the range of 250-500 nm and displayed in Figure 1A.

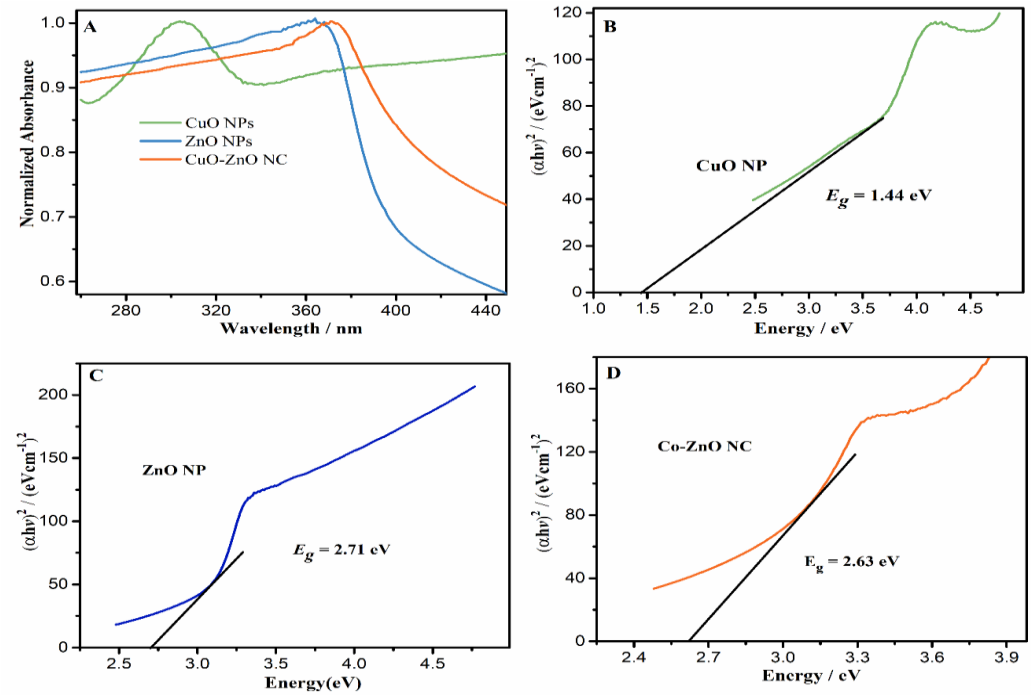

Figure 1. UV-Vis spectrum of CuO NPs, ZnO NPs, and CuO-ZnO NCs synthesized using *Citrus sinensis* fruit peel extract (A); Energy band gap of CuO NPs (B), ZnO NPs (C) and CuO-ZnO NCs (D)

Different absorption maxima for CuO NPs, ZnO NPs, and CuO-ZnO NCs were found at 306, 368, and 372 nm, respectively, as revealed in the UV-Vis spectra of the nanomaterials. The synthesized CuO-ZnO NCs showed a slightly red-shifted absorption edge due to the band gap reduction and this result is corroborated by the previous report [39]. In the UV-Vis spectra, CuO-ZnO also had a wider band, suggesting the production of bigger nanocomposites. This broader band may be due to surface imperfections caused by the bonding of two metal oxides. In contrast, smaller NPs production is indicated by narrower bands in the CuO and ZnO cases [36].

Figures 1B, 1C, and 1D display the optical band gaps of CuO NPs, ZnO NPs, and CuO-ZnO NCs, respectively. Based on the optical absorption spectra, the energy band gap values were calculated using the Tauc relationship, as illustrated by the following equation:

$$(\alpha h\nu)^n = B(h\nu - E_g) \qquad (1)$$

where, α is the linear absorption coefficient, Eg is the energy band gap, *h* is Plank's constant, *v* is photon frequency, B is the proportionality constant associated to the particular material, and n is a constant whose value is 2 for direct transitions and 1/2 for indirect transitions.

The direct band gap energies for CuO NPs, ZnO NPs, and CuO-ZnO NCs are 1.44, 2.71, and 2.63 eV, respectively, based on the Tauc plot (Figures 1B, 1C, and 1D). The outcome demonstrates that the CuO-ZnO NCs' band gap is smaller than that of the ZnO NPs and larger than that of the CuO NPs. Most of the CuO dopants cause a small reduction in the band gap of ZnO NPs, which improves visible light absorption. ZnO NPs without doping exhibit the narrowest band gap.

To identify the functional groups of the synthesized samples, FT-IR analysis was carried out in the region of 4000 - 400 cm^{-1}. Figure 2A displays the FT-IR spectra of CuO, ZnO, and CuO-ZnO nanomaterials that were made using *Citrus sinensis* fruit peel extract. As shown in Figure 2A, broad bands were observed between 3519 - 3464 cm^{-1} for the OPE, CuO-ZnO, ZnO, and CuO nanomaterials, confirming the presence of hydroxyl groups. There is a slight red-shift in the O-H stretching wave number during the synthesis of the nanomaterials, confirming the formation of the nanomaterials. Due to the presence of chemisorbed water, vibrations at around 3478 cm^{-1} were attributed to both symmetric and asymmetric H-O-H stretching vibrations. The C-H stretches in CH_3 and C=O bonds, respectively, are represented by the low intensity bands that were seen at 2818 and 1599 cm^{-1}, respectively. The C=O stretching-induced absorption bands, which arise between 1587 and 1599 cm^{-1}, exhibit a small shift as a result of the NP and NC production. The most significant absorption bands in the FT-IR spectra of CuO, ZnO, and CuO-ZnO nanomaterials were found between 759 and 835 cm^{-1}, which is indicative of the stretching vibrations of the Cu-O and Zn-O bonds. A prior report [40] supports the finding that the absorption bands of metal oxides were below 835 cm^{-1}, which can be attributed to interatomic vibrations.

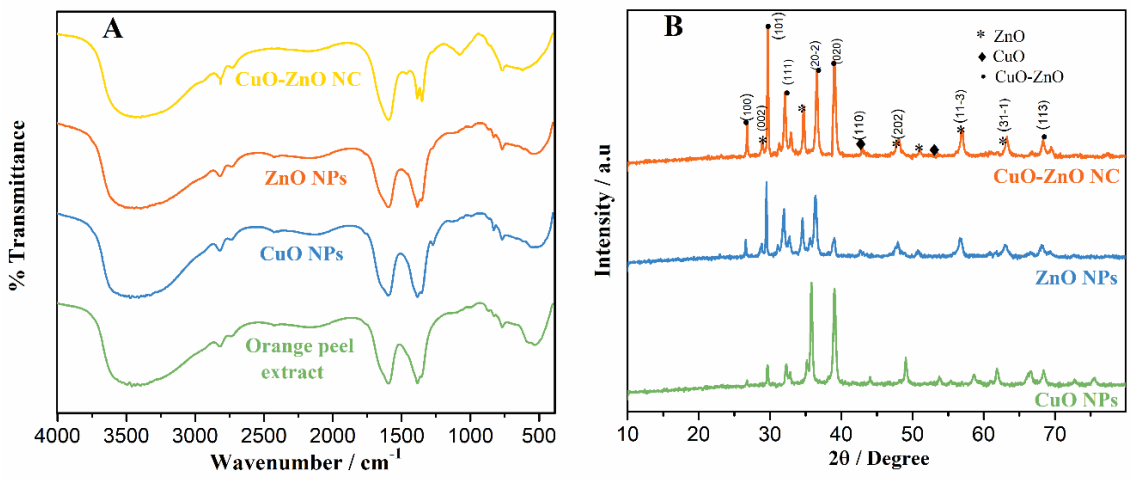

Figure 2. FT-IR spectra of *Citrus sinensis* (Orange) peel extract (OPE), CuO, ZnO, and CuO-ZnO nanomaterials (A); XRD pattern of CuO, ZnO and CuO-ZnO nanomaterials (B)

The fabricated CuO NPs, ZnO NPs, and CuO-ZnO NCs were analyzed by XRD to determine their phase, purity, size, and crystallinity as shown in Figure 2B. The XRD patterns of the ZnO NPs at the 2θ values of 32.58, 35.66, 39.01, 43.96, 58.73, 61.7, 66.4 and 68.08° were indexed as (110), (11-1), (111), (20-2), (020), (202), (022) and (31-1) respectively, corresponding to the hexagonal ZnO phase. Similarly, the diffraction peaks of CuO NPs obtained at the 2θ values of 32.18, 34.45, 36.33, 47.84, 56.68, 63.09, 68.18, and 69.11° indexed as (100), (002),(11-1),(101),(111) (102), (020), (210), (202), and (11-3), respectively were assigned to the monoclinic CuO phase. Moreover, the diffraction peaks of CuO-ZnO NCs observed at the 2θ values of 32.76, 34.4, 36.28, 47.58, 56.62, 62.84, 66.36, 67.98, and 69.14° matched with the ZnO and CuO phases, confirming the formation of CuO-ZnO NCs. However, some diffraction peaks were observed at 26.56 and 29.7°, confirming the presence of impurities of $Zn(OH)_2$ in the synthesized nanomaterials.

The average crystallite size has been calculated by using the Debye-Scherrer formula which is given as follows:

$$D = K\lambda / \beta \cos\Theta \qquad (2)$$

where D is the particle size, λ is the incident x-ray beam's wavelength, Θ is Bragg's diffraction angle, β is the full width at half maximum (FWHM) in radians, and K is a constant that is designated based on parameters linked to the crystallite's structure; usually assumed to be 0.9.

The average crystallite size was determined using Scherrer's formula for the first three intense peaks: (100), (002), and (101) for ZnO; (002), (101), and (111) for CuO NPs; and (100), (101), and (111) for the CuO-ZnO NCs. The average crystallite sizes of CuO NPs, ZnO NPs and CuO-ZnO NCs were found to be 32.2, 31.7, and 35.5 nm respectively. The low-intensity peaks in the XRD patterns of ZnO NPs indicate small size and low crystallinity. The crystallite sizes and trend patterns observed in these three nanomaterials (CuO–ZnO > CuO > ZnO)

appeared to be in good agreement with the result reported for nanomaterials synthesized from *Dovyalis caffra* leaf extract [41].

SEM was used to examine the surface morphologies of the produced CuO NPs, ZnO NPs, and CuO-ZnO NCs. The SEM pictures of the nanomaterials made using *Citrus sinensis* fruit peel extract are displayed in Figure 3.

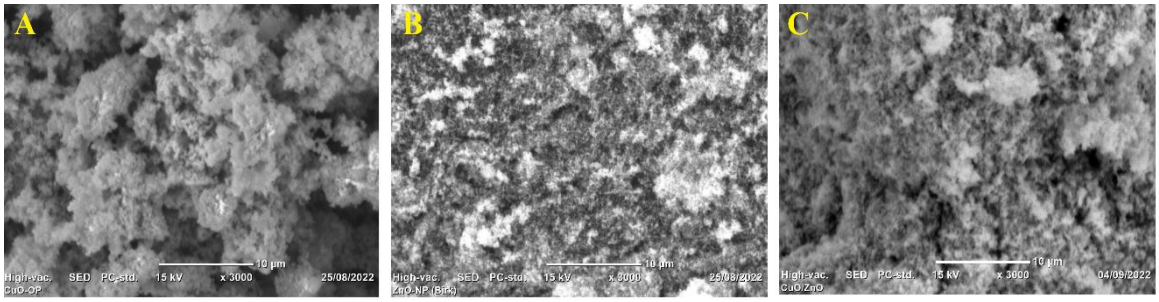

Figure 3. SEM images of the prepared CuO NPs (A), ZnO NPs (B) and CuO-ZnO NCs (C)

CuO NPs and ZnO NPs were primarily found in spherical clusters with a few nano-rod-like structures, according to the SEM images, whereas CuO-ZnO NCs were detected in plate-like morphology. However, when the NPs are joined to form aggregates of various sizes and shapes as a result of the evolution or adsorption of significant volumes of gas, tiny SEM pictures reveal that the CuO-ZnO NCs appear spongy. These nanomaterials' (CuO, ZnO, and CuO-ZnO) trend morphologies (shape, roughness) are consistent with those from earlier research [35].

3.3. Voltammetric determination of H_2O_2 using the synthesized CuO-CPE, ZnO-CPE and CuO-ZnO-CPE

Voltammetric behavior of H_2O_2 was examined at CuO-CPE, ZnO-CPE and CuO-ZnO-CPE in 0.3 M phosphate buffer solution (PBS) at pH 3 using linear sweep voltammetry (LSV).

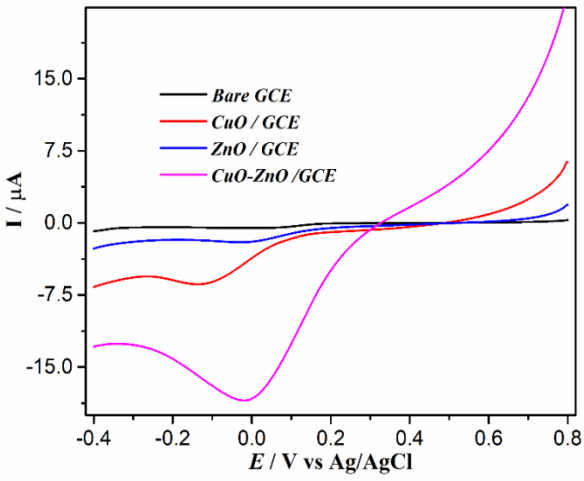

Figure 4. LSV of UCPE and modified electrodes with 5 µM H_2O_2 in 0.1 M pH 3.0 PBS

As shown in Figure 4, H_2O_2 exhibited different voltammetric behaviors at different electrodes. H_2O_2 showed no reduction at UCPE. Very weak reduction current response was observed at ZnO-CPE and CuO-CPE. However, enhanced reduction current response was obtained at CuO-ZnO-CPE. The higher reduction current of H_2O_2 at CuO-ZnO-CPE is more attributed to the higher active surface area of CuO-ZnO NCs present on the surface of modified CPE, which implies that the electron transfer rate was significantly improved.

3.4. Optimization of experimental conditions

3.4.1. Effect of pH and scan rate

Tested in the pH range of 1.8 to 5.0, the impact of pH on the electrochemical detection of H_2O_2 at CuO-ZnO-CPE is displayed in Figure 5A. From 1.8 to 3.0, the cathodic peak current rises as pH rises. However, the reduction peak current of H_2O_2 started to drop as the pH increased more. Therefore, pH 3.0 was determined to be the ideal pH for H_2O_2 determination at CuO-ZnO-CPE.

At various scan rates, the impact of scan rate on the electrochemical behavior of H_2O_2 was also examined. Using 5 µM H_2O_2 in 0.1 M PBS of pH 3.0 at CuO-ZnO-CPE, the LSV corresponding to H_2O_2 reduction was observed at different scan rates ranging from 20 to 140 mVs^{-1}. As the scan rate increases, Figure 5B illustrates that the H_2O_2 reduction current increases. As per the regression equation, $I = 14.5v^{1/2} + 12.1$ and $R^2 = 0.997$, the result likewise showed a direct association between the reduction peak currents and the square root of scan rates (inset of Figure 5B). This demonstrates that the process of H_2O_2 reduction at CuO-ZnO-CPE is diffusion-regulated.

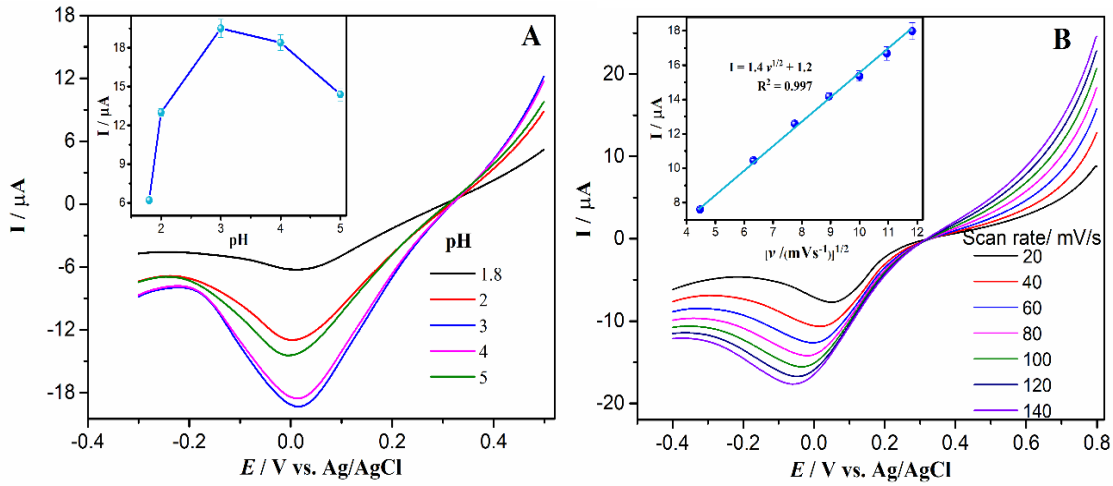

Figure 5. LSVs of CuO-ZnO-CPE containing 5 µM H_2O_2 at various pH values (Inset: Current vs pH) (A); LSV response for the CuO-ZnO-CPE of H_2O_2 at various scan rates in 0.1 M PBS of pH 3.0 (Inset: I vs $v^{1/2}$ plot) (B)

3.4.2. Determination of H_2O_2 at CuO-ZnO-CPE

The effect of varying H_2O_2 concentration at CuO-ZnO-CPE was studied by LSV. As the concentration of H_2O_2 increases, the cathodic peak currents also increase as shown on Figure 6A. A linear relation was observed between concentration of H_2O_2 and reduction peak current values from a concentration range of 0.5 µM to 200 µM (Figure 6B). The computation of the limit of detection (LOD) yielded a value of 0.32 µM (3σ/m), where m represents the slope of the calibration curve and σ represents the standard deviation of seven blank measurements in 0.1 M PBS. Table 2 presents a summary of the findings of a comparison between the analytical performance of the suggested electrode and other reported electrodes.

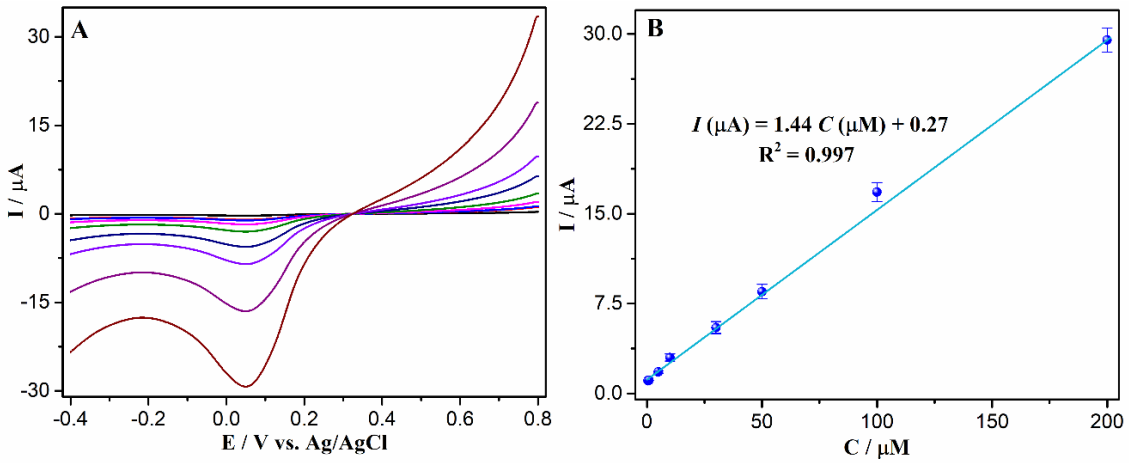

Figure 6. LSV response of CuO-ZnO-CPE at different concentrations of H_2O_2 (0.5-200 µM) in 0.1 M PBS of pH 3.0 at the scan rate of 100 mVs^{-1} (A); Plot of peak current *vs*. concentration (B)

Table 2. Comparison between the developed method and other reported methods for the detection of H_2O_2

Electrode	**Method**	**LOD(µM)**	**Linear range (µM)**	**Ref.**
Type 304 stainless steel electrode	ECL	0.076	0.1 - 1000	[42]
	Amperometry	20	50 - 7330	[43]
AgNPs/ polyethylenimine/GCE	CV	1.66	2 - 1000	[44]
C doped ZnO/GCE	SWV	6.25	50 - 981	[45]
Graphene/Co_3O_4/GCE	CV	1.27	10 - 200	[15]
MoS_2/GCE	CV	1.13	10 - 100	[46]
WS_2/GCE		0.88	10 - 90	[47]
MnO_2/Zeolitic imidazolate framework-8/GCE	LSV	0.157	10–100	[48]
CuO-ZnO-CPE	LSV	0.32	0.5 - 200	This work

3.5. Real sample analysis

The standard addition method was used to recover H_2O_2 under optimal conditions from commercial antiseptic wound wash, which is labeled to contain 3% w/v H_2O_2 using reported method [14]. This was done in order to assess the suggested electrode for practical applications. The wound wash sample was purchased from pharmaceutical drug store. The sample solution was diluted and spiked into the PBS buffer (pH 3.0). Then, 20, 25, and 30 µM H_2O_2 standard solution was ejected to the spiked buffer separately. Finally, the concentration was determined by the standard addition method using the bare and modified GCEs. The measurement was repeated 3 times and the percentage recovery of H_2O_2 was calculated to evaluate the accuracy of the method. Table 3 displays the range of recoveries that were obtained, which falls between 90 and 98.2%. This suggests that the assay that was designed can accurately determine H_2O_2 in real samples analysis.

Table 3. Amount of H_2O_2 detected in the wound wash hydrogen peroxide using the developed method

Sample	Spiked (µM)	Found (µM)	Recovery %	RSD (%)
Wound wash	0	7.5	-	
	20	27.7	98	4.87
	25	32.5	90	1.53
	30	37.5	90.1	1.33

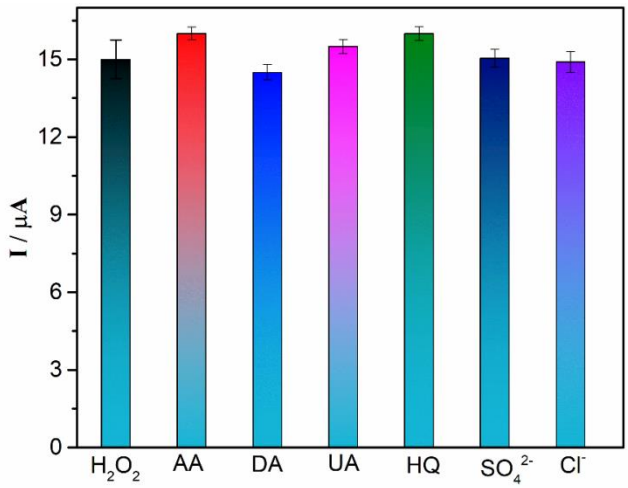

Figure 7. Effect of different interferences on the electrochemical determination of H_2O_2

3.6. Effect of interfering species

To assess the suitability of the devised technique and the specificity of CuO-ZnO-CPE in determining H_2O_2, the impact of potential interfering agents was examined under ideal

circumstances. Various species that cause interference were introduced into the solution that contains 10 μM of H_2O_2. The study of the effect of species that can interfere with the determination of H_2O_2 on the cathodic peak current value was conducted using the CuO-ZnO-CPE. Figure 7 illustrates a number of potential interfering compounds that may coexist with H_2O_2, including ascorbic acid (AA), dopamine (DA), uric acid (UA), hydroquinone (HQ), sulfate ion (SO_4^{2-}), and chloride ion (Cl^-) in 0.1 M PBS at pH 3.0. Under ideal circumstances, these compounds have very little effect on the measurement of 10 μM H_2O_2. The reason for the usage of the aforementioned interferences is that, together with H_2O_2, they are most frequently found in clinical and pharmacological applications [49].

3.7. Stability and reproducibility of CuO-ZnO CPE

Through a series of repeated tests, the reproducibility and storage stability of CuO-ZnO CPE were examined. Using an optimal experimental approach, the electrode response to 5 μM of H_2O_2 was measured to determine the electrode stability after 20 days at room temperature. It was observed that around 95.5% of the initial value was preserved by the current response. Three electrodes were prepared under the same modification circumstances in order to study the electrode reproducibility for CuO-ZnO CPE. To assess the reproducibility, 5 μM of H_2O_2 was determined three times using each electrode. After several measurements, it was determined that there had been no appreciable changes to the electrode characteristics and that the analytical signal was fairly reproducible across the three electrodes. After computation, the relative standard deviation (RSD%) was discovered to be 0.9%. The reproducibility of the data was confirmed by the fact that the sensitivities stayed constant at all three modified electrodes. The low standard deviation (SD) and relative standard deviation (RSD%) results show that the suggested approach has good accuracy and high precision.

4. CONCLUSION

The CuO-ZnO NCs were synthesized by a green approach employing an aqueous extract of Citrus sinensis fruit peel and characterized using UV-Vis, FT-IR, XRD, and SEM analysis. The synthesized CuO-ZnO NCs' UV-Vis spectra revealed a slightly red-shifted, broader absorption band, confirming the nanocomposite's formation. The creation of the nanomaterial is further supported by the slightly red-shifted absorption frequency for O-H stretching shown in the FT-IR spectra. The CuO-ZnO nanocomposite was found to have larger sizes than the CuO and ZnO nanoparticles, according to the XRD pattern. The produced CuO-ZnO NCs were discovered to have a plate-like shape, according to SEM analysis, whereas the CuO and ZnO NPs were primarily made up of clusters with spherical morphologies. The CPEs modified with CuO-ZnO nanocomposite showed a higher reduction current of H2O2 in the voltammetric analysis of H2O2 using the LSV method than the CPEs modified with CuO and ZnO nanoparticles and the unaltered CPEs. Under ideal experimental conditions, CuO-ZnO-CPE

demonstrated a superior response for H_2O_2 detection. There was no cathodic peak for dissolved oxygen reduction at CuO-ZnO-CPE, however a cathodic peak for H_2O_2 reduction was seen at roughly 0.0 V. Using the LSV approach, the active modified electrode's sensing efficiency was evaluated. The sensor demonstrated improved performance in detecting H_2O_2 over a broad linear concentration range (0.5-200 μM) with a low limit of detection (0.32 μM). Additionally, the fabricated electrode demonstrated improved operational stability, reproducibility, and compatibility for analysis of real samples. The findings of this study reveal that the proposed technique can be used to detect H_2O_2 in a variety of samples from the biological, medicinal, and environmental domains.

Acknowledgments

The authors would like to acknowledge Jimma University School of Graduate Studies and Department of Chemistry for funding and material support.

Declarations of interest

The authors declare no conflict of interest in this reported work.

REFERENCES

[1] R. Kulkarni, S. Kunwar, R. Mandavkar, J.H. Jeong, and J. Lee, Nanomaterials 10 (2020) 2034.
[2] Y.K. Hsu, Y.C. Chen, and Y.G. Lin, Appl. Surf. Sci. 354 (2015) 85.
[3] S.A. Kitte, B.D. Assresahegn, and T.R. Soreta, J. Ser. Chem. Soc. 78 (2013) 701.
[4] W. Jia, M. Guo, Z. Zheng, T. Yu, E.G. Rodriguez, Y. Wang, and Y. Lei, J. Electroanal. Chem. 625 (2009) 27.
[5] M.R. Jones, and K. Lee, Microchem. J. 147 (2019) 1021.
[6] X. Yu, Y. Gong, W. Xiong, M. Li, J. Zhao, and Y. Che, Anal. Chem. 91 (2019) 6967.
[7] M. Wang, S. Qiu, H. Yang, Y. Huang, L. Dai, B. Zhang, and J. Zou, Chemosphere 270 (2021) 129448.
[8] W. Lu, Y. Sun, H. Dai, P. Ni, S. Jiang, Y. Wang, Z. Li, and Z. Li, Sens. Actuator B: Chem. 231 (2016) 860.
[9] T. Chen, L. Tian, Y. Chen, B. Liu, and J. Zhang, Nanoscale Res. Lett. 10 (2015) 252.
[10] R.M. Trujillo, D.E. Barraza, M.L. Zamora, A. Cattani-Scholz, and R.E. Madrid, Sensors 21 (2021) 2204.
[11] N. Sobahi, M. Imran, M.E. Khan, A. Mohammad, M.M. Alam, T. Yoon, I.M. Mehedi, M.A. Hussain, M.J. Abdulaal, and A.A. Jiman, Materials 16 (2023) 2770.
[12] T.N. Pham, N. Van Cuong, N.X. Dinh, H. Van Tuan, V.N. Phan, N. Thi Lan, M.H. Nam, T.D. Thanh, V.D. Lam, N. Van Quy, T.Q. Huy, M.H. Phan, and A.T. Le, J. Electrochem. Soc. 168 (2021) 026506.

[13] E. Blanco, L. Vázquez, M. del Pozo, R. Roy, M.D. Petit-Domínguez, C. Quintana, and E. Casero, Bioelectrochem. 135 (2020) 107581.
[14] N.F. Atta, S.A. Abdel Gawad, A. Galal, A.A. Razik, and A.R.M. El-Gohary, J. Electroanal. Chem. 881 (2021) 114953.
[15] P. Murugan, A.K. Sundramoorthy, R.D. Nagarajan, R. Atchudan, R. Shanmugam, D. Ganapathy, S. Arya, A.A. Alothman, and M. Ouladsmane, J. Nanomater. 2022 (2022) 1-10.
[16] L. Fernández, J. Alvarez-Paguay, G. González, R. Uribe, D. Bolaños-Mendez, J.L. Piñeiros, L. Celi, and P.J. Espinoza-Montero, Front. Chem 10 (2022) 884050.
[17] A. Gorgij, H. Ahmar, and L. Adlnasab, Iran. J. Anal. Chem. 8 (2021) 50.
[18] R. Sha, A. Basak, P.C. Maity, and S. Badhulika, Sens. Actuators Rep. 4 (2022) 100098.
[19] C.E. Cheng, S. Tangsuwanjinda, H.M. Cheng, and P.H. Lee, Coatings 11 (2021) 936.
[20] F. Buarki, H. AbuHassan, F. Al Hannan, and F.Z. Henari, J. Nanotechnol. 2022 (2022) 5474645.
[21] T. Shahwan, S. Abu Sirriah, M. Nairat, E. Boyacı, A.E. Eroğlu, T.B. Scott, and K.R. Hallam, Chem. Eng. J. 172 (2011) 258.
[22] P. Salgado, K. Márquez, O. Rubilar, D. Contreras, and G. Vidal, Appl. Nanosci. 9 (2019) 371.
[23] Z. Yuhong, W. Zhong, P. Feng, and F. Li, Braz. J. Pharm. Sci. 52 (2016) 781.
[24] F. Chutrakulwong, and K. Thamaphat, Green Process. Synth 12 (2023) 20230070.
[25] S. Rajendrachari, and B.E.K. Swamy, Phys. Chem. Res. 8 (2020) 1.
[26] E. Turunc, Euro. J. Sci. Techno. (2021) 550.
[27] P.S. Ganesh, S.Y. Kim, S. Kaya, and R. Salim, Sci. Rep. 12 (2022) 2149.
[28] J. Tashkhourian, M.R.H. Nezhad, J. Khodavesi, and S. Javadi, J. Electroanal. Chem. 633 (2009) 85.
[29] B. Niu, B. Yao, M. Zhu, H. Guo, S. Ying, and Z. Chen, J. Electroanal. Chem. 886 (2021) 115121.
[30] N.B. Ashoka, B.E.K. Swamy, H. Jayadevappa, and S.C. Sharma, J. Electroanal. Chem. 859 (2020) 113819.
[31] S. Deepa, B.E.K. Swamy, and K.V. Pai, J. Electroanal. Chem. 879 (2020) 114748.
[32] G. Yashni, A. Al-Gheethi, R.M.S. Radin Mohamed, N.V. Dai-Viet, A.A. Al-Kahtani, M. Al-Sahari, N.J. Nor Hazhar, E. Noman, and S. Alkhadher, Chemosphere 281 (2021) 130661.
[33] T. Gonfa, S. Teketle, and T. Kiros, Cogent Food Agric. 6 (2020) 1853867.
[34] G.A. Ayoola, H.B. Coker, S.A. Adesegun, A.A. Adepoju-Bello, K. Obaweya, E.C. Ezennia, and T.O. Atangbayila, Trop. J. Pharm. Res. 7 (2008) 1019.
[35] A.G. Bekru, L.T. Tufa, O.A. Zelekew, M. Goddati, J. Lee, and F.K. Sabir, ACS Omega 7 (2022) 30908.

[36] E.E. Elemike, D.C. Onwudiwe, and M. Singh, J. Inorg. Organomet. Polym. 30 (2020) 400.
[37] T. Nemomsa, S.A. Kitte, E.T. Woldemariam, and T.H. Fereja, Acta Chemica IASI 28 (2020) 1.
[38] E. Hosseinzadeh, A. Foroumadi, and L. Firoozpour, Inorg. Chem. Commun. 147 (2023) 110243.
[39] Z. Shehu, E. Abba, D.W. Lamayi, K.P. Yoriyo, Z.A. Abubakar, Z.N. Kenneth, Z. Usiju, and A. Abubakar, J. Pharm. Res. Int. 32 (2020) 31.
[40] K.W. Aga, M.T. Efa, and T.T. Beyene, ACS Omega 7 (2022) 10796.
[41] J.O. Adeyemi, D.C. Onwudiwe, and A.O. Oyedeji, Molecules 27 (2022) 3206.
[42] S.A. Kitte, W. Gao, Y.T. Zholudov, L. Qi, A. Nsabimana, Z. Liu, and G. Xu, Anal. Chem. 89 (2017) 9864.
[43] S.A. Kitte, M.N. Zafar, Y.T. Zholudov, X. Ma, A. Nsabimana, W. Zhang, and G. Xu, Anal. Chem. 90 (2018) 8680.
[44] K.T. Kim, and D.S. Park, Catalysts 10 (2020) 1416.
[45] M.A. Rashed, M. Faisal, F.A. Harraz, M. Jalalah, M. Alsaiari, and S.A. Alsareii, J. Electrochem. Soc. 168 (2021) 027512.
[46] V.S. Haritha, A. Vijayan, S.R. Sarath Kumar, and R.B. Rakhi, Mater. Lett. 301 (2021) 130258.
[47] V.S. Haritha, S.R. Sarath Kumar, and R.B. Rakhi, Mater. Sci. Eng. B 285 (2022) 115932.
[48] K. Ahmad, W. Raza, A. Alsulmi, and H. Kim, Colloids Surf. A: Physicochem. Eng. 674 (2023) 131937.
[49] Mihailova, V. Gerbreders, M. Krasovska, E. Sledevskis, V. Mizers, A. Bulanovs, and A. Ogurcovs, Beilstein J. Nanotechnol. 13 (2022) 424.